Collisions in a liquid fluidized bed

Alicia Aguilar-Corona [a,c,d], Roberto Zenit [b,*], Olivier Masbernat [a,d]

[a] Université de Toulouse, INPT-UPS, Laboratoire de Génie Chimique, 4, allée Emile Monso BP 44362, 31030 Toulouse Cedex 4, France
[b] Instituto de Investigaciones en Materiales, Universidad Nacional Autónoma de México, Apdo, Postal 70-360, México D.F. 04510, Mexico
[c] Facultad de Ingeniería Mecánica, Universidad Michoacana de San Nicolás de Hidalgo, Francisco J. Mujica s/n C.P. 58030, Morelia-Michoacán, México
[d] CNRS, Fédération de recherche FERMAT, FR 3089 1, Allée du Professeur Camille Soula, 31 400 Toulouse, France

A B S T R A C T

Collisional phenomena in a solid–liquid flow were studied in terms of two parameters: the collision frequency and the coefficient of restitution. Experimental measurements of these parameters were conducted inside a liquid fluidized bed by particle tracking in an index-matched array. Collision detection was based on the use of a peak acceleration threshold of the instantaneous speed of colored tracers. The measurements of collision frequency were compared with the theoretical expression derived from the kinetic theory for granular flow (KTGF). The normal and tangential restitution coefficients were measured from the trajectories before and after contact for both particle–particle and particle–wall collisions. A comparison with previous theoretical and experimental works is presented and discussed.

1. Introduction

A particulate flow is composed of two phases: a dispersed solid phase and continuous fluid (gas or liquid) phase. These flows are frequently found in many industrial applications and also in various natural phenomena. Despite their prominence, a general understanding of their mechanical behavior is still not widely accepted. One of the issues that make the physical description of particulate flows to be difficult is the effect of the solid phase. Early on, Bagnold (1954) discussed that particles affect the rheology of such flows in two different manners depending on the role that particles played in the flow. If the viscous effects are dominant, the effect of the particles is to 'simply' modify the bulk viscosity of the flow (the so-called macro-viscous regime); on the other hand, if the effect of interstitial fluid is negligible, the particles collide against themselves (collisional regime) and the behavior can be described using a kinetic theory approach. Although recently the experimental measurement of Bagnold have been questioned (Hunt et al., 2002), his original arguments remain paradigmatic.

In particular, for the case of solid–liquid particulate flows it is unclear when can the collisional effects can be considered dominant. When the fluid has a finite viscosity, the hydrodynamic force diverges as the distance between surfaces vanishes (Brenner, 1961). However, Joseph et al. (2001) showed that if the particle has sufficient inertia, a collision can occur. The dominant dimensionless group that determines if the particle is to collide or not is the Stokes number, which is defined as

$$St = \frac{\rho_p V d_p}{9\mu_f} \tag{1}$$

where ρ_p, V and d_p are the density, velocity and diameter of the particle, respectively, and μ_f is the fluid viscosity. The number 9 in the denominator is kept by convention. This number compares the particle inertia with viscous forces. Additionally, when the elasticity of the solid particle is considered, the elasticity parameter needs to be considered (Davis et al., 1986).

There have been several attempts to use the kinetic theory for granular flows (KTGF), which is based on the hypothesis that particles interact through collisions, to study particulate flows (Simonin, 1991; Ding and Gidaspow, 1990; Koch, 1990). The relevance of statistical models issued from KTGF for the description of the particular case of a liquid fluidized bed has been demonstrated for the case of large but finite Stokes numbers (Gevrin et al., 2008; Aguilar, 2008) ($10 < St < 100$). The pertinence of this type of kinetic theory model was shown by Aguilar (2008) for the prediction of the mean energy level evolution as a function of the solid fraction. In these models, however, collisions are described in the same way as in a dry granular media, i.e. at infinite Stokes number, where the influence of the interstitial fluid is not accounted for. The liquid fluidization of large particles lies in the transition regime between low Stokes number regime, where hydrodynamic forces are dominant and large Stokes number controlled by collisions. Moreover, solid–liquid flow numerical simulations will always need realistic (repulsive) interaction models between particles when the inter-particle distance becomes smaller than a single grid cell (Joseph and Hunt, 2004).

In order to fully elucidate the validity of these models, a direct assessment of the collisional motion within a solid–liquid flow

* Corresponding author. Tel.: +52 55 5622 4593.
E-mail address: zenit@servidor.unam.mx (R. Zenit).

needs to be conducted. This is the main purpose of the present investigation. To do this we have decided to use a liquid fluidized bed. In such a system, a bed of solid particles is suspended by an upward liquid flow. Beyond a certain liquid flow rate threshold, the particles are fluidized as the bed expands but their mean velocity remains close to zero. In this state, however, the particles have a significant agitation which is a caused by either collisions or hydrodynamic forces. Hence, particle–particle and particle–wall collisions are inherent of a fluidized bed description. They influence the overall agitation level through the transport properties (collisional viscosities) and they contribute to the fluctuating kinetic energy dissipation rate. Also, collisions in a fluidized bed play an important role in transfer phenomena. Contact between particles and walls may also have consequences as erosion and debris sedimentation or film depositions and thickening on solid surfaces (Ben-Ammar et al., 1992; Nore, 1992; Del Pozo et al., 1993).

Two main parameters characterize collisions in a liquid-fluidized bed: the collisional frequency (f_{coll}) and the normal restitution coefficient (e_c). The determination of these parameters has been the subject of multiple studies in the past, most of them dedicated to the normal restitution coefficient. Joseph et al. (2001) studied normal particles collisions against immersed walls for a large range of Stokes numbers. Their results suggest that the normal restitution coefficient is an increasing function of the Stokes number (based on the impact velocity, $St = \rho_p V_{im} d_p/(9\mu_f)$). Joseph and Hunt (2004) addressed the case of oblique collisions. They were able to generalize the dependency of the normal restitution coefficient as a function of the Stokes number based upon the normal component of the wall impact velocity ($St = \rho_p V_{N,im} d_p/(9\mu_f)$), ranging between 30 and 4000. More recently, Yang and Hunt (2006) measured binary normal collisions between spheres of different diameters and confirmed the normal restitution coefficient evolution as a function of Stokes number based on the relative velocity component projected in the direction defined by their center of mass. Their results are in excellent agreement with those corresponding to particle–wall interaction (normal or oblique). Moreover, all these experimental investigations showed the existence of a critical Stokes number (i.e. a critical impact velocity). Below this threshold, collisions are dampened by the interstitial liquid and do not lead to a rebound ($e_c = 0$). This critical Stokes number is about 10 ± 5.

Based on a dampened mass-spring model, Legendre et al. (2006) proposed a simple correlation for the normal restitution coefficient:

$$\frac{e_c}{e_{c\,\max}} = \exp(-35/St) \tag{2}$$

where e_{cmax} is the maximum (dry) coefficient of restitution. In this case, the Stokes number was based on the normal "unperturbed" impact velocity, V_∞, and on the particle added mass ($\rho_{eff} = \rho_p + 0.5\rho_f$). This correlation (Eq. (2)) covers an important number of experimental data found in the literature for collisions of solid and fluid particles with solid walls submerged in liquids. Legendre et al. also proposed a correlation for the collision contact time, which is proportional to the contact time in vacuum (Hertzian contact) but increases slightly with Stokes number. For solid particle–wall collisions in a liquid, the contact time remains small compared to the relaxation time of the particle. This result shows that the collision can be described like a trajectory discontinuity, using of a coefficient of restitution.

The collision frequency measurement in fluidized beds has received less attention than the restitution coefficient. Del Pozo et al. (1993) have measured the collision frequency in both gas and liquid fluidized beds, using an electro-chemical particle gauge, a technique initially intended to measure the mass transfer between phases. Although quantitative measurements cannot be obtained from this study, it is clear that the collision frequency is an increasing function of the solid fraction, which reaches a maximum at the minimum fluidization velocity (i.e. for the largest solid fraction in a fluidized regime). The first investigations on this subject were performed by Zenit et al. (1997), who measured the granular pressure at the wall for a large range of operating conditions (solid fractions and Stokes numbers), by means of a piezo-electric sensor. These data have been largely validated by other studies (Gevrin et al., 2008; Buyevich, 1997; Wang and Ge, 2005); however, the collision frequency and its evolution with solid fraction was not reported. Buffière and Moletta (2000), using the technique developed by Zenit et al. (1997), measured the collision frequency at the wall in a three-phase (gas–liquid–solid) fluidized bed. They observed an increasing evolution of the frequency as a function of the solid fraction which showed a maximum at about 20%. This surprising (and counter-intuitive) result contradicts the evolution predicted by the kinetic theory and rests, to date, unexplained.

In the present work, we have measured both the normal coefficient of restitution and the collision frequency within a liquid fluidized bed. We opted for a liquid fluidized bed as a model system for liquid–solid flows because the mean velocity of the solid phase is zero; this feature allows us to study the fluctuating motion of particles. The objective of this study is to measure "simultaneously" the collision frequency in the core of the bed as a function of the solid fraction, as well as the normal restitution coefficient between the particles and the bed walls. Instead of a parametric study of the restitution coefficient in a well controlled arrangement, our intention is to verify the applicability of such a concept in a liquid–solid flow by obtaining *in situ* measurement. In other words, we would like to verify that the time and velocity scales of the random particle motion in the fluidized bed are compatible with the notion of the restitution coefficient during a collision (trajectory discontinuity). This concept is relevant for high Stokes number flows (dry media); however, for finite but moderate Stokes numbers the validity of such concept still needs to be verified experimentally. Such validation has not been reported in the literature to date.

2. Experimental set-up

2.1. Particles and fluid

Calibrated 6 mm Pyrex beads were fluidized by a concentrated aqueous solution of Potassium Thiocyanate (KSCN, 64% w/w). At 20 °C, the fluid and the particles have the same refractive index ($n_D \simeq 1.474$), so that a tagged particle can be tracked individually in a nearly transparent suspension. In fact, due to the non-homogeneous structure of the beads, there is a slight refractive index mismatch: the particles are never completely invisible within the solution. This fact limits the range of particle concentration that can be investigated by optical techniques; however, we took advantage of this slight mismatch to measure the bed height and to track unmarked particles trajectories. Particle and fluid properties are reported in Table 1. Due to the moderate values of the density difference and of the fluid viscosity, the particle Reynolds number at terminal velocity ($Re_t = V_\infty d\rho_f/\mu_f$) is high but the Stokes number (defined as $St_t = (\rho_p/\rho_f)Re_t/9$) is of O(100). The values of these parameters are reported in Table 2. Additionally, this particle size makes the images analysis (particle tracking) to be more

Table 1
Fluid and particle properties at 20 °C.

Pyrex beads	$d_p = 6$ mm	$\rho_p = 2230$ kg/m^3	$n_D = 1.474$
KSCN solution 64% w/w	$\mu_f = 3.8 \times 10^{-3}$ Pa s	$\rho_f = 1400$ kg/m^3	$n_D = 1.4744$

Table 2
Fluidization parameters.

d_p (mm)	V_∞ (m/s)	Re_t	St_t	n
6	0.226	500	88.4	2.41

precise, as explained below. The fluidization law of this system was identified by measuring the bed height as a function of the fluidization velocity. The exponent n of the well-known Richardson–Zaki relation (Richardson and Zaki, 1954) is equal to 2.41, which is the expected value in this range of particle Reynolds number.

2.2. The fluidized bed

The experimental set-up of the fluidized bed is shown schematically in Fig. 1. It is composed of a 8 cm diameter glass column of 60 cm in height. A flow homogenization section was mounted at the bottom of the column, composed of a honeycomb panel, a fixed bed of particles and layers of synthetic foam. Thanks to this system, the particles occupy the whole space of the fluidized bed and no stationary recirculation loop is detected, suggesting a homogeneous fluidization.

In order to avoid optical distortion due to the wall curvature, a glass square section box was mounted around the column and filled with the fluidizing liquid. The KSCN solution is pumped from a 30 L tank; it flows upward in the column and is sent back to the tank. Its temperature is controlled by a secondary water loop and a heat exchanger. The particle volume fraction, α_p, was inferred from the measurement of the bed expansion.

2.3. Particle tracking technique

The analysis of collisions was achieved by 2-D trajectography of particles within the fluidized bed. Images were recorded with a

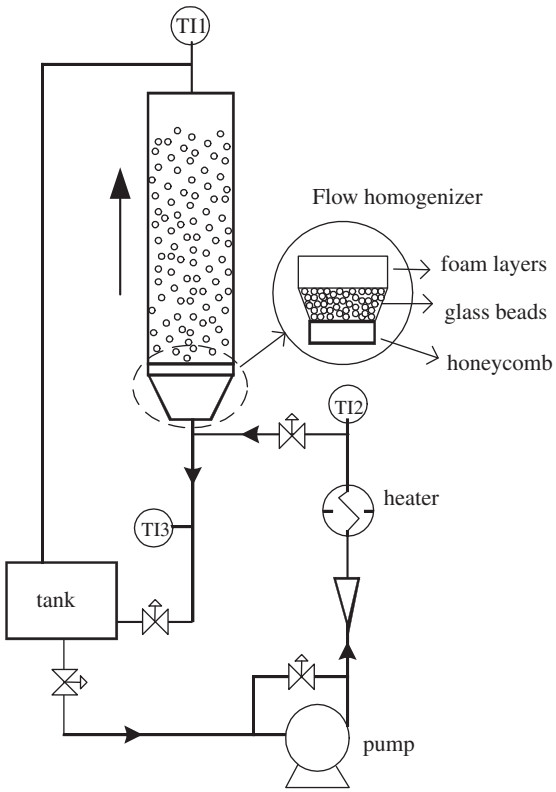

Fig. 1. Scheme of the liquid fluidized bed.

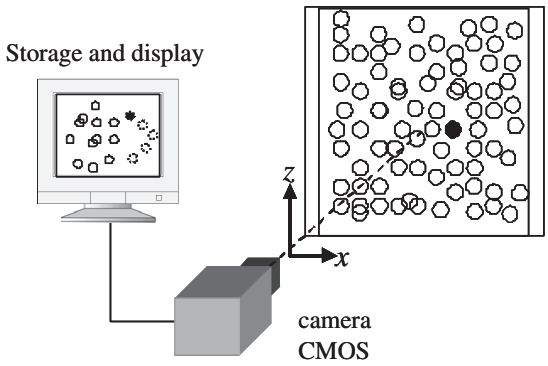

Fig. 2. Scheme of the particle tracking technique.

high speed camera (Photron APX) equipped with a CMOS sensor. The test zone is an area of 8×8 cm^2 using the maximum resolution (1000×1000 pixels). A black colored particle was introduced in the bed and its trajectory was recorded at 500 frames per second. Fig. 2 shows a scheme of the arrangement. To ensure that the tracer particle remained 'focused' while moving across the cross-section of the fluidized bed, the depth of field was widen by placing the camera at a relatively large distance from the fluidized bed (about 2 m).

The collision frequency was determined from the trajectory of a single colored particle, following the vertical (z) and horizontal (x) directions of the flow. The particle position was determined on each image by means of image processing: gray level thresholding followed by a binarization. The center of mass of the tracer particle in the binary image was located. The instantaneous velocity and acceleration vectors of the center of mass of the particle were derived using a central difference scheme. Note that with the present optical arrange, the out-of-the-plane motion (y-direction) of the particle cannot be measured. Therefore, the motion in this direction cannot be registered or measured. Figs. 3 and 4 illustrate the image sequence during a collision and their corresponding acceleration signal, respectively. Clearly, the collision induces a peak in the acceleration signal of the tracer particle. A threshold criterion was applied to the acceleration intensity to detect a collision event. Using this criterion, the mean collision frequency was measured for six different mean solid fractions (α_p = 0.11, 0.16, 0.2, 0.25, 0.3 and 0.4).

The wall–particle restitution coefficient was determined from the trajectories of unmarked particles, before and after impact with the bed walls. The collisions were initially detected visually on few seconds of video recordings. Each collision event was extracted from the sequence and a contrast adjustment process was applied to improve the detection of the contour of the impacting particle. The particle circumference and its geometric center were then computed. The particle–wall collision analysis was performed for three different concentrations (α_p = 0.11, 0.20 and 0.25). Only the events where the particle–wall collision was not detectably perturbed by other particles were taken into account (this is the reason why this part of the study was limited to 25% of mean solid fraction). Fig. 5 shows a wall collision sequence of a transparent particle: before the collision (Fig. 5a and b), at the moment of the contact, Fig. 5c, and after the collision (Fig. 5d and e).

3. Theoretical background: oblique collisions

Oblique collisions pose a greater challenge to be described physically than normal collisions (Johnson, 1985) because, in addition to the normal contact, two different processes can occur in the tangential direction: rolling or sliding. In sliding, the relative

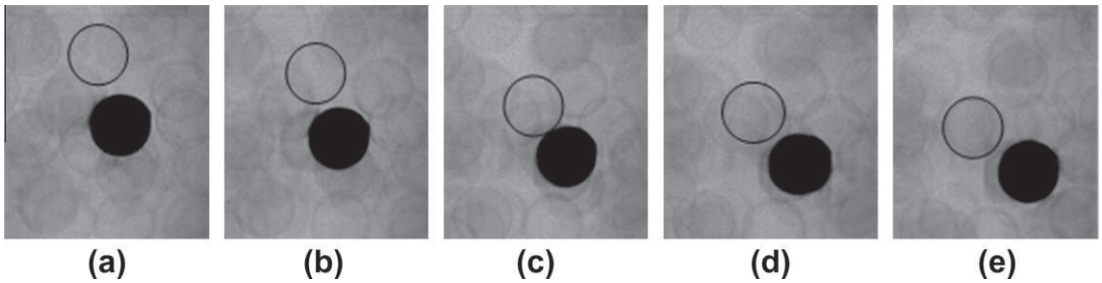

Fig. 3. Image sequence of a particle collision (time intervals of 0.02 s): (a and b) before collision, (c) during collision and (d and e) after a collision. $\alpha_p = 0.16$. The black circle shows the particle colliding with the marked particle.

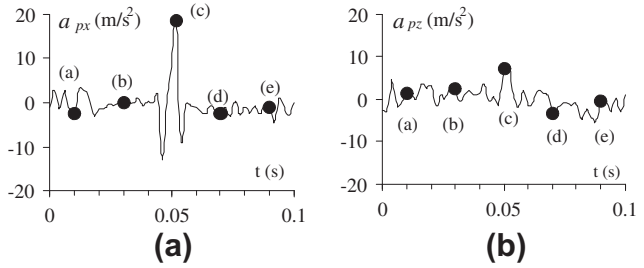

Fig. 4. Acceleration signals of a particle trace. The solid circles correspond to the images in Fig. 3: (a) and (b) correspond to the x and z directions, respectively.

velocity of the contacting surfaces is nonzero; for rolling, the surfaces at the point of contact do not move with respect to each other. While the normal contact can be described by Hertzian theory, the description of tangential contact is much more complex. Mindlin (1949) showed that while gross-slip and rolling can appear, in most cases both happen in the contact area during the collision process (the so-called micro-slip). To account for the loading history that occurs during a collision Maw et al. (1976) proposed a method to calculate the process of a contact in which micro-slip occurs. They divide the contact region in a series of equi-spaced concentric circles, in which either slip and stick occurs. In slip regions, the tangential traction is given by the friction coefficient and the local normal contact pressure distribution. In stick regions, a tangential displacement is prescribed. Walton proposed a model (Walton, 1993) for which the whole process of an oblique elastic collision can be described through three measurable parameters. The model is relatively simple and retains the most important aspects of this process. Hence, to explain the nature of the collisions within the fluidized bed the parameters of Walton's model were inferred using our measurements. Below, we make a brief summary the measurements and how the parameters are calculated.

Fig. 6 shows the reference frame used for the calculation of the particle trajectory and velocity. The origin of the reference frame was placed at the position of the particle center of mass at the

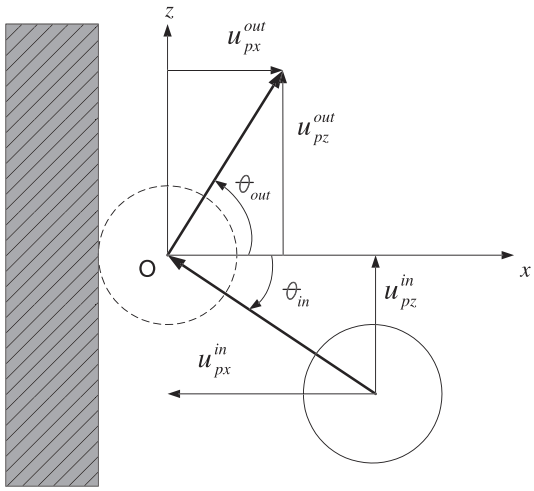

Fig. 6. Scheme of the reference frame for the velocity angles and components during a particle–wall rebound in the fluidized bed.

instant of contact (corresponding to the instant of sign reversal of the normal velocity component). The normal velocity before the impact is taken to be positive and, consequently, the normal rebound velocity is always negative. The impact tangential velocity component sign is always positive, no matter its direction with respect to the vertical axis (Oz). The rebound and impact angles are referred with respect to the wall normal, always positive and less than $\pi/2$. The collision frequency and wall–particle restitution coefficient were obtained using the same video recordings; hence, both measurements correspond to the same flow conditions.

Once the velocity components (before and after the impact) are determined, the rebound parameters can be evaluated. The normal restitution coefficient is defined as the ratio of the algebraic values of the normal velocity components after and before the rebound:

$$e_c = -\frac{u_{px}^{out}}{u_{px}^{in}} \tag{3}$$

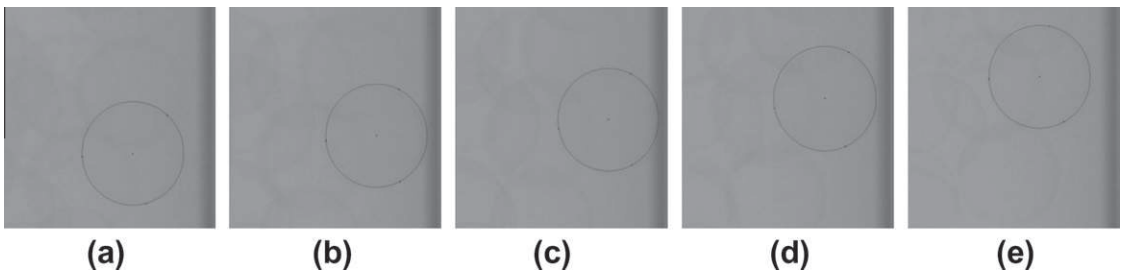

Fig. 5. Non-marked particle identification during a rebound with the wall ($\alpha_p = 0.1$). Images contrast was slightly increased. The time interval between images is 0.04 s. (a and b) Before collision; (c) contact; (d and e) after collision.

The angles θ_{in} and θ_{out} (with respect to the wall normal) are then obtained from the velocity components as:

$$\theta_{in} = \arctan\left(\frac{|u_{pz}^{in}|}{|u_{px}^{in}|}\right) \tag{4}$$

$$\theta_{out} = \arctan\left(\frac{|u_{pz}^{out}|}{|u_{px}^{out}|}\right) \tag{5}$$

Considering the contact model of Walton (1993), we can calculate the rotational restitution coefficient, β, which is defined as:

$$\beta = -\frac{u_{pz}^{out}}{u_{pz}^{in}} \tag{6}$$

If we consider the effective angles of incidence ($\Psi_{in} = \tan\theta_{in}$) and rebound ($\Psi_{out} = e_c \tan\theta_{out}$), Eq. (6) can be written as

$$\beta = -\frac{\Psi_{out}}{\Psi_{in}} \tag{7}$$

The coefficient β varies in the range $[-1,+1]$. $\beta = -1$ corresponds to a rebound without slip $\left(|u_{pz}^{out}| = |u_{pz}^{in}|\right)$, and $\beta = 0$ to a rolling particle after contact. A positive value of β implies that the bead recoils after the collision.

The last parameter of Walton's model is the coefficient of sliding friction, η_f (note that the original notation was modified to avoid confusion with the liquid viscosity). Following the work of Joseph and Hunt (2004), the friction coefficient η_f, for homogeneous solid spheres, is given by:

$$\eta_f = \frac{2(1+\beta)}{7(1+e_c)}\Psi_{in} \tag{8}$$

Hence, from our measurements of the incident and rebound velocities and their respective angles, the three contact parameters of the oblique contact model (e_c, β, and η_f) can be calculated. It is important to note that, in addition to Walton's model, there are other interpretations of the rotational restitution coefficient. For instance, Brilliantov and Poeschel (2004) refer to the parameter β as a tangential coefficient of restitution, because in its calculation the rotational velocities of the particle (before and after the contact) are not considered.

4. Results

4.1. Restitution coefficient

The random character of the particle–wall collision in the bed and the rather tedious manual pre-processing, make the acquisition of a large set of data to be impractical. Moreover, it is not possible to choose *a priori* the range of values of the incident impact velocity (and hence the value of the Stokes number). However, it is known that the impact velocity is correlated, in average, to the mean agitation level in the bed, which is a continuously decreasing function of the solid fraction (Aguilar, 2008). Therefore, the tests performed at different concentrations will have, in average, different impact velocities. The impact velocity decreases as the concentration increases. This expected evolution is, of course, valid for the absolute value of the relative impact velocity, the impact angle remains random.

Some examples of trajectories following the normal (indexed x) and the tangent to the wall (indexed z) are reported in Fig. 7. The instants before and after the collision correspond to negative and positive times, respectively. From these trajectories, the impact velocity components and were calculated over a time interval ranging between 10 and 20 ms (before and after the rebound). To be significant, these velocities must be nearly constant within this time interval. This time interval must therefore be larger than the

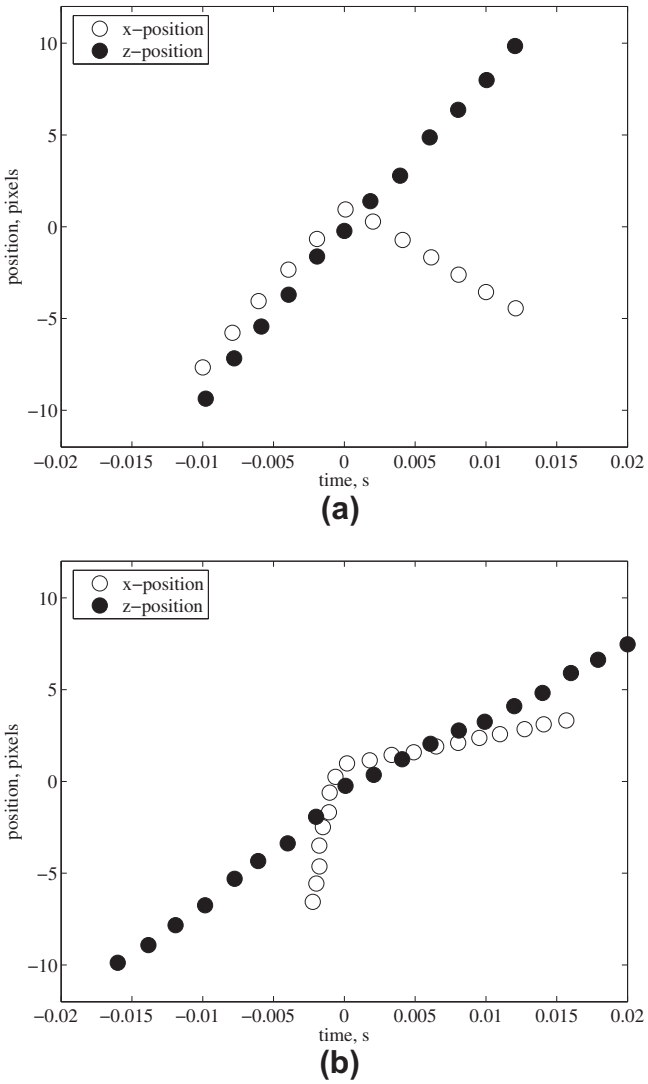

Fig. 7. Time evolution of the particle position during the collision (a) $\alpha_p = 0.11$ and (b) $\alpha_p = 0.2$.

time at which the lubrication film develops and smaller than the characteristic time of the velocity fluctuation of the particle. Fig. 8 shows the cumulative mean particle velocity for two concentrations in the horizontal and vertical components. If one considers that the particle "sees" the wall at a distance of the order of one tenth of its radius, (i.e. 0.3 mm or 4 pixels on the images), for a 6 mm particle at a speed of 0.1 m/s, the time at which the film develops can be estimated to be about 3 ms before the rebound, a value smaller than the time interval considered. In addition, the smallest Lagrangian time scale of the fluctuating motion of the particle within the bed is approximately 70 ms, according to Aguilar (2008), supporting the assumption of a constant velocity during a time interval of the approach–contact–rebound process. However, it is possible that within this temporal window, the incident particle velocity may fluctuate. In this case, the measurement was either rejected or the impact velocity was calculated over a smaller time interval.

The determination of the velocity after the rebound is more arbitrary. The contact time or rebound time can be estimated from the relationship given by Legendre et al. (2006), which predicts for this range of Stokes number a contact time twice as large as the Hertz contact time, about 100 μs in our case. In comparison with the acquisition frequency from the trajectories (500 Hz), the

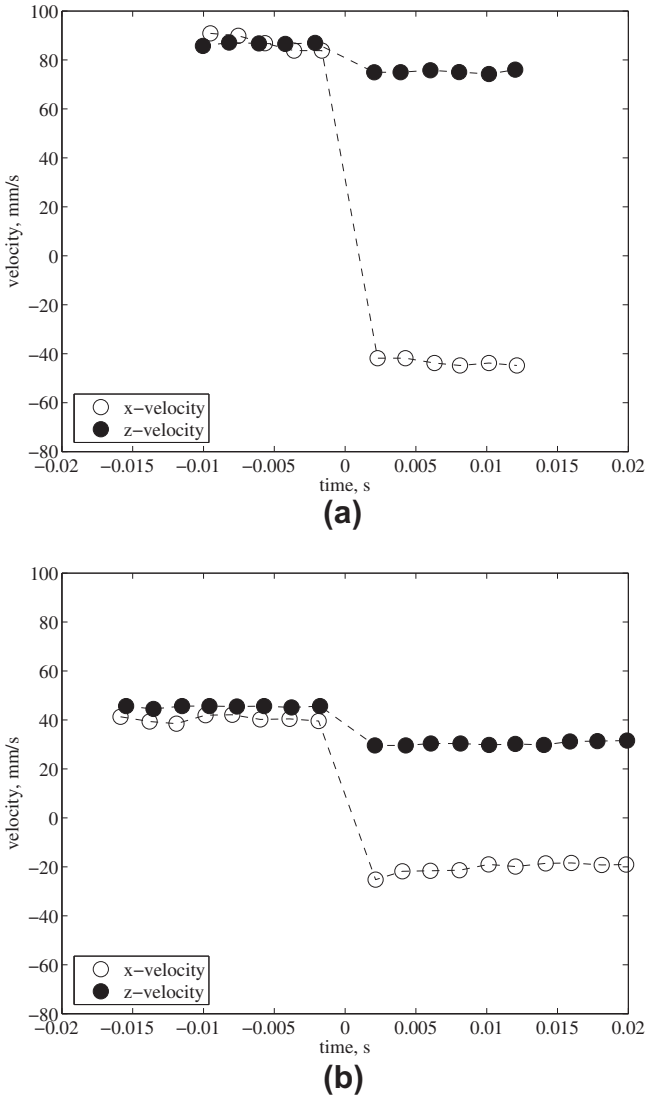

Fig. 8. Cumulative mean of the horizontal (x) and vertical (z) particle velocity components during the rebound (a) $\alpha_p = 0.11$ and (b) $\alpha_p = 0.20$.

contact time can be disregarded. At the moment of rebound, the effect of the liquid velocity fluctuations (susceptible of interacting with the particle during the collision) and the presence of large scale motion, (which generate velocity gradients at the vicinity of the wall) were not evaluated. As for the impact velocity, the cumulative time average of both velocity components after the rebound and was calculated over a time window ranging between 10 and 20 ms. When a plateau of ±10% of the value at the current time step was reached, the value was accepted as the rebound velocity. Fig. 8 illustrates the cumulative mean particle velocity components at two distinct solid fractions in the bed. These curves show that in the range of flow parameters investigated (in terms of solid fraction and Stokes number), collisions in a liquid fluidized bed can be described using the concept of coefficient of restitution.

A total of fourteen particle–wall impact trajectories were processed (3 for $\alpha_p = 0.11$, 6 for $\alpha_p = 0.2$ and 5 for $\alpha_p = 0.25$), corresponding to values of the normal impact velocity,u_{px}^{in}, between 0.02 and 0.1 m/s. The Stokes number (defined in Eq. (1)), based on u_{px}^{in}, St_{in}, ranges between 10 and 35.

The normal and tangential velocities after the collision (u_{px}^{out} and u_{pz}^{out}, respectively) are reported in Fig. 9 as a function of their respective components before the impact, u_{px}^{in} and u_{pz}^{in}. Note that u_{px}^{out} and u_{pz}^{out} are both increasing functions of the impact velocity and that the energy dissipation during the collision leads to smaller values of the velocity after the collision (compared with the impact velocity). The tangential components after the rebound are nearly unchanged, while their corresponding normal component is smaller (in absolute value) than the normal component at impact. Additionally, the curves in Fig. 9a and b suggest that the normal velocity component vanishes after the rebound for a correspondingly nonzero impact velocity. This trend confirms the existence of a critical velocity below which the collision is dampened by the film, hindering the rebound.

The numerical values of the contact and rebound parameters (described in Section 3), for all the fourteen wall-rebound trajectories, are reported in Table 3. The first two columns show the solid fraction and Stokes number at impact, respectively. It can be observed that the measured rebound parameters are independent of the solid phase fraction. We can, therefore, infer that the particle trajectories processed before and after the rebound were not affected by neighboring particles, a necessary condition for the significance restitution coefficient measurement.

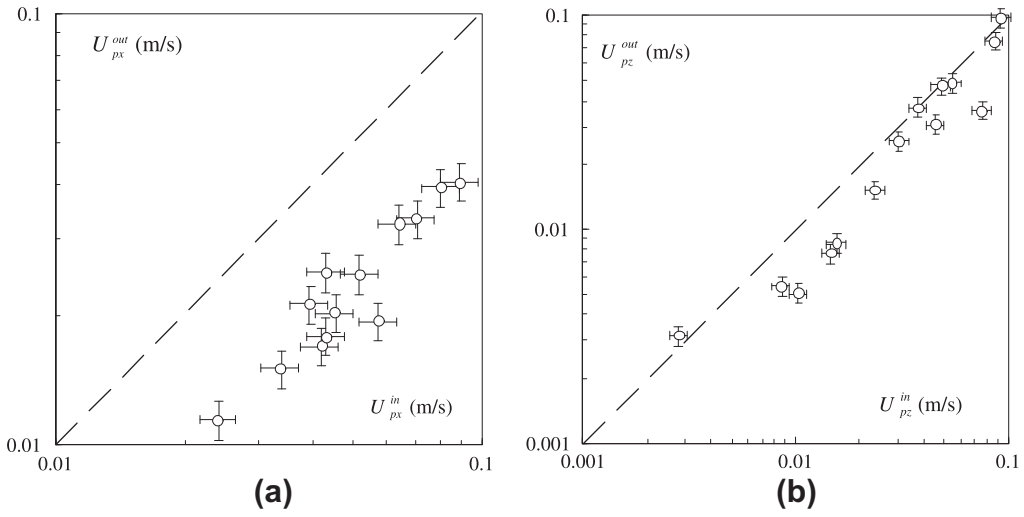

Fig. 9. Velocity components after collision as a function of impact components. (a) Normal velocity, (b) tangential velocity.

Table 3
Rebound parameters measured before (in) and after (out) impact.

α_p	St_{in}	e_c	θ_{in}	θ_{out}	Ψ_{in}	Ψ_{out}	β	η_f
0.11	34.9	0.454	44.1	61.8	0.969	0.845	−0.872	0.0244
0.11	13.2	0.446	23.4	27.1	0.432	0.229	−0.529	0.0403
0.11	31.4	0.491	49.2	67.9	1.04	1.208	−1.045	−0.0099
0.2	20.2	0.480	16.8	19.1	0.271	0.166	−0.551	0.0262
0.2	17.7	0.449	46.9	66.6	1.07	1.036	−0.968	0.0067
0.2	16.4	0.404	41.7	65.4	0.779	0.882	−0.990	0.0018
0.2	15.5	0.537	49.0	55.6	1.150	0.783	−0.681	0.0683
0.2	9.4	0.474	72.3	72.3	3.134	1.485	−0.474	0.3197
0.2	14.0	0.221	4.5	22.0	0.091	0.089	−1.141	−0.0026
0.25	22.4	0.339	10.2	14.5	0.18	0.088	−0.487	0.0197
0.25	27.5	0.474	18.6	24.6	0.337	0.217	−0.642	0.0234
0.25	16.8	0.586	51.9	62.5	1.275	1.125	−0.882	0.0271
0.25	16.8	0.415	11.3	17.0	0.200	0.126	−0.632	0.0149
0.25	24.9	0.510	25.7	38.3	0.503	0.403	−0.839	0.0147

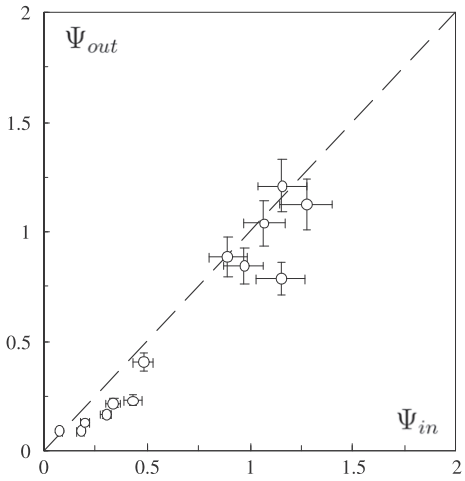

Fig. 10. Effective rebound angle, Ψ_{out} as a function of its corresponding incident value, Ψ_{in}.

The values for Ψ_{out} are reported as a function of Ψ_{in} in Fig. 10. We observe that the values of Ψ_{out} are always smaller, but close to Ψ_{in}. Hence, for all these collisions we can infer that a rather limited slip took place. The difference between Ψ_{out} and Ψ_{in} is quantified by β-values ranging between 0 and −1, and η_f-values different from zero. There are no β values near zero; hence, there was no rolling during these experiments after the impact. The value of β is always negative (in general smaller than 0.5 in absolute value), indicating that no recoil occurred after the collision. Values of β greater than 1 probably result from experimental uncertainty.

In Fig. 11a, β has been plotted as a function of the incident angle, θ_{in}. Despite a rather large scatter of the data, a decreasing trend of β between −0.5 and −1 can be observed for a range of θ_{in} comprised between 10° and 60°. Only two points seem to deviate significantly from this trend (filled symbols). The corresponding evolution of η_f is reported in Fig. 11b. No particular tendency can be identified for this case: the values of η_f fluctuates between 0 and 0.05. Two values, corresponding to the two filled circles in Fig. 11a, are distinctively larger (η_f =0.068 for θ_{in} = 49° and η_f = 0.32 for θ_{in} = 72.3°; this latter value does not appear on the graph). It is interesting to compare our results to those of Joseph and Hunt (2004) for glass and steel beads of a diameter twice larger than the Pyrex beads of our study, in liquid solutions of comparable viscosity (between 1 and 5 centipoises). They observed significant differences on the evolution of β and η_f (hardly visible on the dimensionless curves of Fig. 10) that seem correlated to particle roughness. Rough

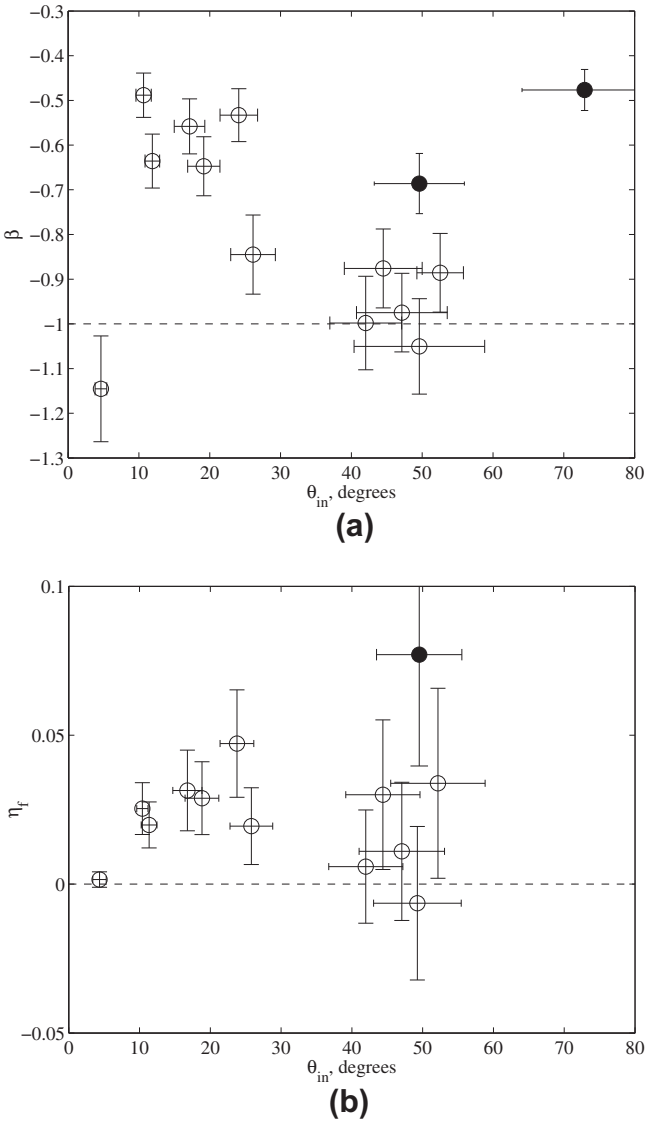

Fig. 11. (a) Rotational restitution coefficient, β, and (b) friction coefficient, η_f, as a function of impact angle θ_{in}. The filled symbols indicate collisions for rough particles.

particles (glass beads in their study) correspond to smaller values of β (in absolute value), hence to larger values of η_f, which grow with the incident angle, between 0 and 0.2 when θ_{in} varies between 0° and 70°. Conversely, between 0° and 70°, smooth particles (steel beads) exhibit a sharp decrease of β to −1 and η_f values are ranging between 0 and 0.035, independently of the incidence angle θ_{in}. This comparison indicates that our results are very good agreement with those reported by Joseph and Hunt, in particular for the case of smooth particles (η_f values being very close in both studies). The two filled symbols in Fig. 11a would, therefore, correspond to rougher particles and consequently to larger η_f values. However, the particle roughness was not evaluated directly in the present study.

The evolution of the normal restitution coefficient e_c as a function of Stokes number based on impact normal velocity, St_{in}, has been plotted in Fig. 12 for the measurements shown in Table 3. An important scatter of e_c is observed (between 0.2 and 0.6) for a limited variation of the Stokes number, comprised between 10 and 35.

In Fig. 12, the correlation by Legendre et al. (2006) (dotted line) and the mean trend from the experiments of Joseph and Hunt

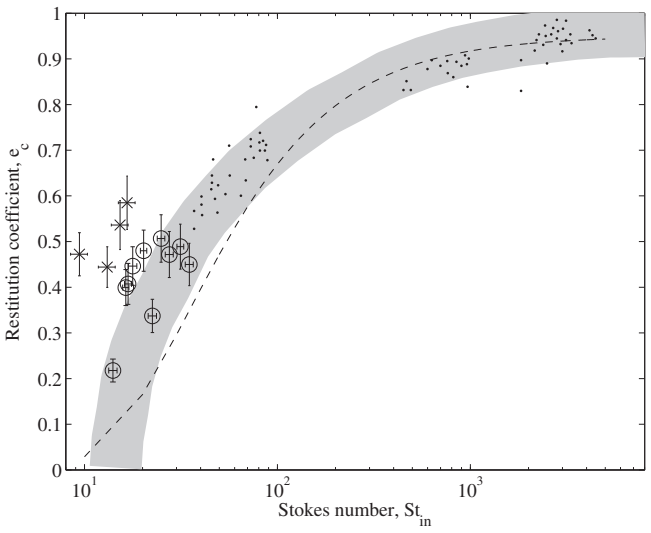

Fig. 12. Normal restitution coefficient as a function of the impact Stokes number (St_{in}). Experimental data from this study: (○), values for which $\eta_f < 0.027$; (×), values for which $\eta_f > 0.027$; black dots, experimental data from Joseph and Hunt (2004) (oblique collisions); gray band: experimental trend from Joseph et al. (2001) (normal collisions); dotted line: correlation of Legendre et al. (2006).

(2004) (gray band) are also shown. Our experimental results are in very good agreement with those of Joseph and Hunt but are slightly above the correlation of Legendre et al. Even if the dispersion of the values of the normal restitution coefficients is generally expected to be large (Joseph et al., 2001), that shown in Fig. 12 is even greater (even if the size of the error bars is taken into account). This trend is probably due to the fact that in this range of Stokes number, the decrease of the normal restitution coefficient is rather steep. Some studies (Joseph et al., 2001; Yang and Hunt, 2006; Barnocky and Davis, 1988) predict a critical Stokes number (below which there is no rebound) of order 10. However, if we consider the values of e_c corresponding to the smallest values of the friction factor η_f (smaller than 0.027) the dispersion of data in Fig. 12 is reduced (black circles). Clearly, these points closely follow the mean trend obtained by Joseph and Hunt (2004). This result can be explained by the fact that the largest values of η_f correspond to small rebound angles (with respect to the normal). Consequently a larger normal restitution coefficient is obtained. This trend is also observed in Fig. 12, where our data is also compared to those of Joseph and Hunt (2004) for oblique collisions (black dots) and those of Joseph et al. (2001) for normal collisions (gray band). We can conclude that our measurements in the fluidized bed confirm the previously observed trend for normal and oblique collisions within this range of Stokes numbers, for low roughness particles (or more precisely, for $\eta_f < 0.027$).

4.2. Inter-particle collision frequency

Collision frequency was measured in the core of the bed from the analysis of the high frequency signal of a marked particle. Since the particle experiences a sharp velocity variation as a result of a collision, a criterion based on the intensity of the instantaneous acceleration signal was chosen to detect particle contacts. Fig. 13 shows two velocity signals $u_{pi}(t)$, following the vertical z and transverse x directions. Visual inspection of the video and time signals confirm the correspondence between the collision events and the acceleration peaks. It was also observed that the amplitude of the acceleration peaks is always larger in the vertical direction compared to the horizontal component. In order to establish a single collision criterion, the absolute value of acceleration was normalized using its maximal value in a given trajectory:

$$\gamma_i = \frac{|a_i(t)|}{|a_{imax}|} \tag{9}$$

where a_i is the acceleration in the i direction, calculated as the time derivative of the velocity signal $u_{pi}(t)$.

The γ_i signal is shown in Fig. 14a and b, following the vertical and horizontal axis, respectively, as a function of time. This

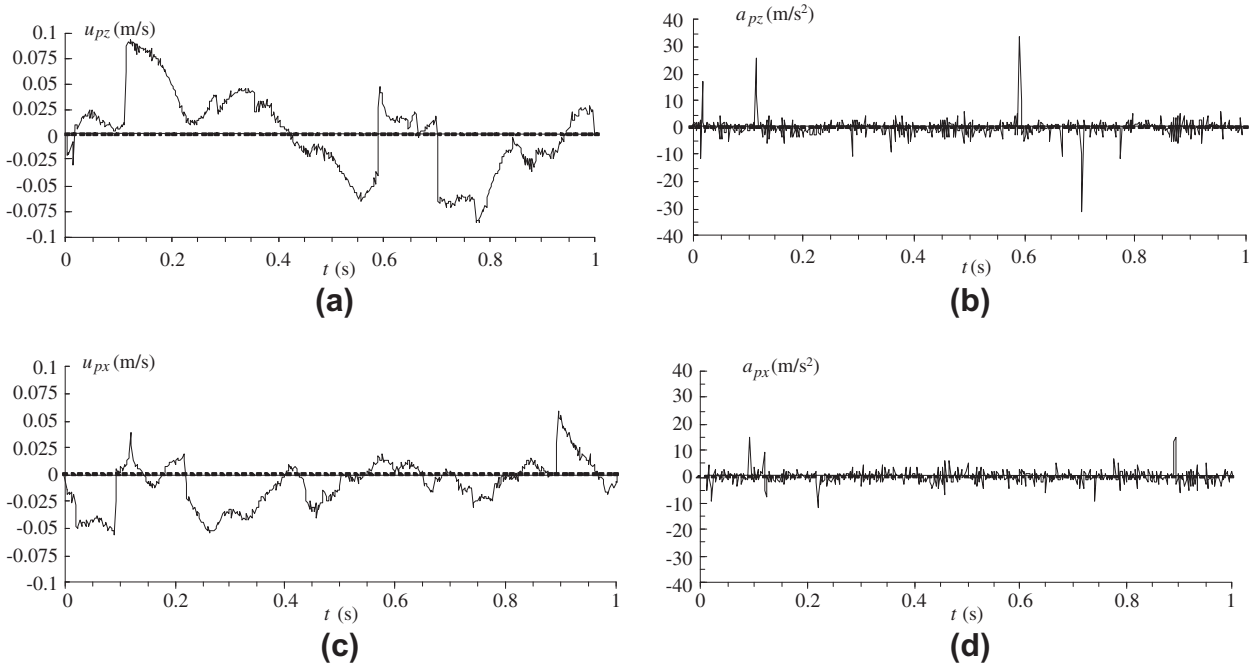

Fig. 13. Instantaneous velocity and acceleration signals. (a and c) Velocity in the z and x directions, respectively. (b and d) Acceleration in the z and x directions, respectively. $\alpha_p = 0.16$.

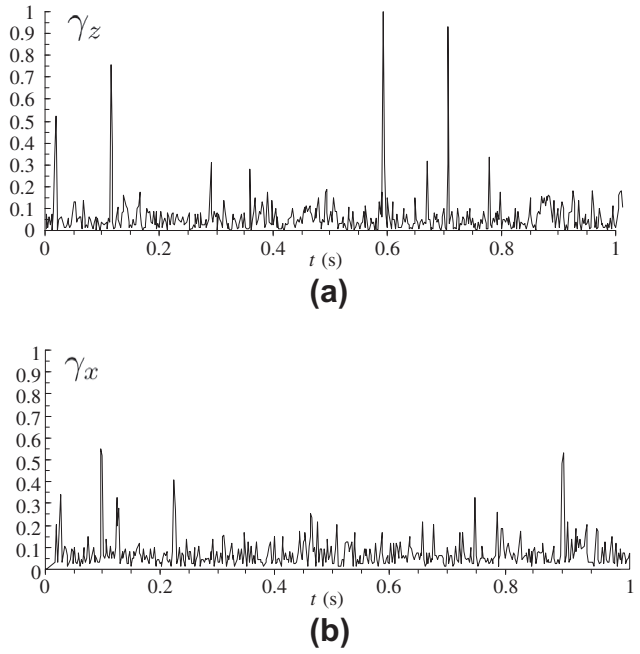

Fig. 14. Instantaneous signals of the normalized absolute acceleration (a) along z (b) along x (c) arithmetic mean of. Letters x and z indicate the collisions visually observed in the video film along x and z, respectively. The number of observed collisions (11) correspond to a threshold close to 0.2 ($\alpha_p = 0.16$).

normalized acceleration allows for the definition of a single threshold for collision detection, γ_{coll}. The arithmetic average of acceleration, $\gamma = (\gamma_x + \gamma_z)/2$, is presented in Fig. 14c. For each recorded trajectory, the collisions frequency f_{coll} was deduced dividing the number of values exceeding the threshold γ_{coll} by the total recording time.

In addition, the collision events were detected individually and counted visually from the video film. These collision events are depicted in Fig. 14c by the characters x and z, indicating the preferential contact orientation during the collision. There is good agreement between the total number of visually detected collisions over the entire recording (11 in this case) and the value obtained considering a threshold $\gamma_{coll} = 0.2$. The transparent particle that collides with the marked one can be identified using the video recordings. Fig. 15 illustrates the trajectory of the marked particle which corresponds to the signal of Fig. 14c during a time interval comprised between 0.58 and 0.78 s, where three collisions were observed. In Fig. 15, the abscissa and ordinate correspond to the width and height of the visualization field. The perimeter of the transparent colliding particle was drawn in the images and the collision instant is also shown. The arrows show the sense of the motion before collision.

Fig. 16 shows the γ signals obtained for three different concentrations, $\alpha_p = 0.11$, 0.25 and 0.40. It can be observed that the

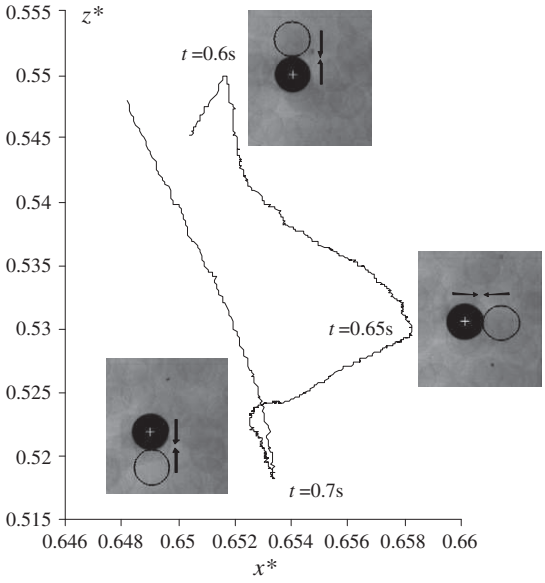

Fig. 15. Particle trajectory and collision events during the time interval $0.58 < t < 0.73$, corresponding to Fig. 14c.

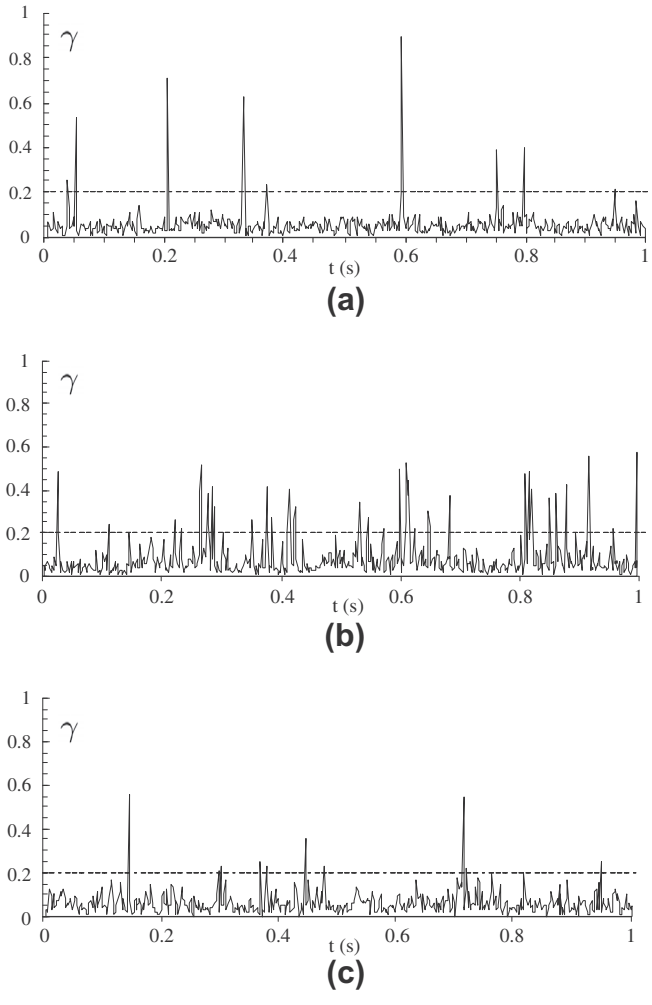

Fig. 16. Time signal of the normalized acceleration. The number of collisions indicated for each graph corresponds to γ values greater than $\gamma_{coll} = 0.2$ (dashed line). (a) $\alpha_p = 0.11$, (b) $\alpha_p = 0.25$, (c) $\alpha_p = 0.40$.

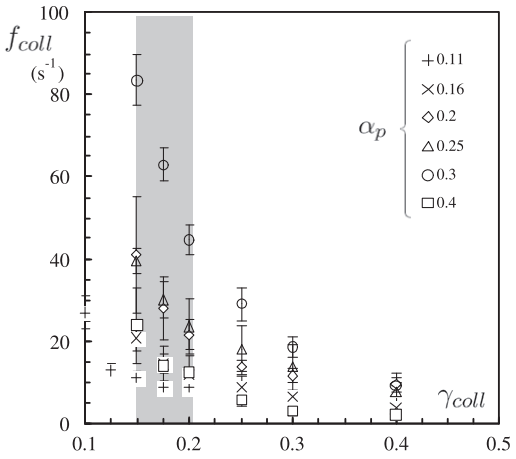

Fig. 17. Collision frequency, f_{coll}, as a function of γ_{coll} for different values of the solid fraction.

number of collisions grows with particle volume fraction for the range between 0.11 and 0.25; surprisingly, the collision count decreases for particle concentrations between 0.25 and 0.4, suggesting the presence of a maximum.

In order to validate the threshold value γ_{coll}, the evolution of the collision frequency, f_{coll}, as a function of the value of the threshold was plotted in Fig. 17 for each solid fraction. The collision frequency is, in fact, a continuously decreasing function of γ_{coll}. Initially, the collision rate decreases rapidly as γ_{coll} increases. In the interval [0.15, 0.2], represented on the graph by a gray band, the rate of change of collision frequency with γ_{coll} is reduced. It can be deduced that a reasonable value of the threshold γ_{coll} lies in this interval.

A dimensionless collision frequency f^*_{coll} can be defined as:

$$f^*_{coll} = \frac{f_{coll} d_p}{\sqrt{\langle \overline{q_p^2} \rangle}} \tag{10}$$

where d_p is the particle diameter and $\langle \overline{q_p^2} \rangle$ is the "small scale" fluctuating kinetic energy of the solid phase in the fluidized bed. The fluctuating kinetic energy can be calculated as

$$\langle \overline{q_p^2} \rangle = \frac{3}{2} \langle \overline{u_p'^2} \rangle \tag{11}$$

where $\langle \overline{u_p'^2} \rangle$ is the particle velocity variance. Aguilar (2008) obtained a measurement of $\langle \overline{q_p^2} \rangle$ considering a very similar arrangement to that described in Section 2.3. The particle trajectory was registered for much longer time periods (up to 200 s) at a frame rate of 30 frames per second. In this manner, the wide range of particle velocity fluctuations was obtained; hence, an accurate measure of the mean kinetic energy was obtained for a range of gas volume fractions. Fig. 18 shows the particle fluctuating kinetic energy as a function of the solid fraction, for the particles used in this study. It can be observed that the kinetic energy of the solid phase decreases with solid fraction. An extensive discussion about these measurements will be reported elsewhere. The reader is referred to Aguilar (2008) for more details.

Considering the measurements of the particle fluctuating kinetic energy, $\langle \overline{q_p^2} \rangle$, the dimensionless collision frequency can be obtained. Fig. 19 shows f^*_{coll} as a function of solid fraction considering a value of $\gamma_{coll} = 0.2$. The figure shows an increase of f^*_{coll} with the concentration up to $\alpha_p = 0.3$; subsequently, the dimensionless collision frequency decreases for larger solid fractions. This result is indeed similar to that observed by Buffière and Moletta (2000) who measured the collision frequency at the wall using a hydrophone.

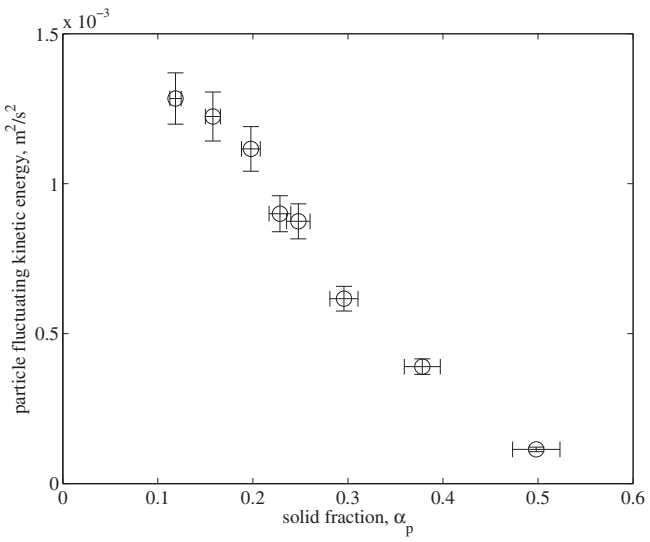

Fig. 18. Fluctuating kinetic energy of the particle phase, $\langle \overline{q_p^2} \rangle$, as a function of solid fraction, α_p, for 6 mm glass beads in the fluidized bed.

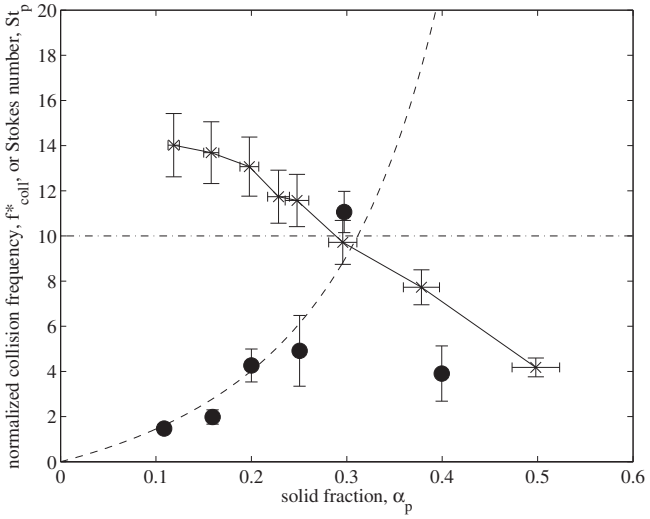

Fig. 19. Dimensionless collision frequency, f^*_{coll}, as a function of the solid fraction, α_p (filled circles). The dotted lines represents the prediction of f^*_{coll} from the KTGF (Eq. (12)). The × symbols show the values of St_p as a function of solid fraction; the horizontal dashed-dotted line shows the critical value of $St_p = 10$.

A prediction of the collision frequency can be obtained from the KTGF (Simonin, 1991):

$$f^*_{coll} = 24\sqrt{\frac{2}{3\pi}} \alpha_p g_o \tag{12}$$

where g_o is the pair correlation function defined as

$$g_o = (1 - \alpha_p/\alpha_{pm})^{-2.5\alpha_{pm}} \tag{13}$$

considering $\alpha_{pm} = 0.64$. The prediction of Eq. (12) is shown in Fig. 19 (dashed line). For concentrations ranging between 0.1 and 0.3, a very good agreement is observed between the prediction and the measurements. In this range of concentrations the evolution of the collision frequency with the solid fraction seems to be validated. In turn, for concentrations larger than 0.3, the theoretical curve continues to increase (because of the rapid growth of the pair correlation function g_o with increasing α_p). This trend is opposite to that followed by the experimental results.

We think that this behavior is due to the detection limit of collisions from the particle acceleration signal. Indeed, these sudden changes of acceleration are present in case of an effective particle rebound, which is the case when the restitution coefficients e_c is different from zero. Dampened collisions are therefore not detected, because they cannot be distinguished from fluctuations due to hydrodynamic interactions. When the solid fraction increases, the total collision frequency may increase but collisions with rebound are less frequent. A simple way to evaluate this effect consists in estimating the Stokes number based on the particle root-mean-square (rms) velocity as a function of the concentration. That is, $St_p = \rho_p \sqrt{\langle \overline{q_p^2} \rangle} d_p/(9\mu_f)$. The comparison of this number with the critical Stokes number (below which the restitution coefficient cancels out) allows us to quantify the collision detection limit for our method. Considering the data shown in from Fig. 18, the value of St_p was calculated and it is plotted in Fig. 19, along with the collision frequency measurements. It turns out that for a solid fraction greater than 0.3, the Stokes number becomes smaller that 10; hence, for such concentrations the Stokes number is below the critical value (Joseph and Hunt, 2004; Joseph et al., 2001; Yang and Hunt, 2006). For such a range of α_p the collision detection criterion based on the acceleration threshold cannot be applied. We can therefore conclude that the present method is limited by the zero-value of the restitution coefficient at high solid phase fraction.

5. Conclusions

The objective of this study was to measure simultaneously the collision frequency and the normal restitution coefficient for particle–wall collisions, within a liquid–solid fluidized bed. The collision frequency was determined using the acceleration signal of a tracer particle, counting the times when the acceleration was larger than a certain threshold value. The normal restitution coefficient was measured analyzing oblique velocity trajectories before and after the impact with the wall from non-marked particles. The principal results of this study can be summarized as follows:

- The normal restitution coefficient concept is pertinent in a liquid fluidized bed, and the evolution of such parameter as a function of the Stokes number, based on the normal impact velocity, is in good agreement with previous experimental data obtained for controlled impact conditions (Joseph and Hunt, 2004; Joseph et al., 2001; Yang and Hunt, 2006). However, it seems that this agreement is limited to collisions where the friction factor η_f is small (of about 0.025), which corresponds to smooth particles. For all other cases, friction and rotation can be therefore neglected.
- The collision frequency is an increasing function of the concentration, correctly represented by the law derived from the KTGF, in an interval for the solid fraction comprised between 0 and 0.3 in our case. At higher concentration, the method used to detect the collisions cannot be used in the present case, due to the dampening of the collisions.
- The good agreement between the measured values of the coefficient of restitution (with previous studies) and the collision frequency (with predictions from KTGF) demonstrates that these concepts are relevant for flows in which the Stokes number is finite but moderate.

Acknowledgments

Alicia Aguilar Corona wishes to thank CONACYT for financial support during the period of her graduate studies. This work has been supported by the research federation FERMaT (FR CNRS 3089).

References

Aguilar, A., 2008. Agitation des particules dans un lit fluidise liquide. Etude exprimentale, Ph.D. thesis, Institut National Polytechnique de Toulouse, Toulouse, France.
Bagnold, R.A., 1954. Experiments on a gravity-free dispersion of large solid spheres in a Newtonian fluid under shear. Proc. Roy. Soc. Lond. A 225, 49–63.
Barnocky, G., Davis, R.H., 1988. Elastohydrodynamic collision and rebound of spheres: experimental verification. Phys. Fluids 31, 501–519.
Ben-Ammar, F., Kaviany, M., Barber, J.R., 1992. Heat transfer during impact. Int. J. Heat Mass Transfer 35, 1495–1506.
Brenner, H., 1961. The slow motion of a sphere through a viscous fluid towards a plane surface. Chem. Eng. Sci. 16, 242–251.
Brilliantov, N.V., Poeschel, T., 2004. Kinetic Theory of Granular Gases. Oxford University Press, Oxford.
Buffière, P., Moletta, R., 2000. Collision frequency and collisional particle pressure in three-phase fluidized beds. Chem. Eng. Sci. 55, 5555–5563.
Buyevich, Y.A., 1997. Particulate pressure in monodisperse fluidized beds. Chem. Eng. Sci. 52, 123–140.
Davis, R.H., Serayssol, J.M., Hinch, E.J., 1986. The elastohydrodynamic collision of 2 spheres. J. Fluid Mech. 163, 479–497.
Del Pozo, M., Briens, C.L., Wild, G., 1993. Particle–particle collisions in liquid–solid and gas–liquid–solid fluidized beds. Chem. Eng. Sci. 48, 3313–3319.
Ding, J., Gidaspow, D., 1990. A bubbling fluidization model using kinetic theory of granular flow. AIChE J. 36, 523–538.
Gevrin, F., Masbernat, O., Simonin, O., 2008. Granular pressure and particle velocity fluctuations prediction in liquid fluidized beds. Chem. Eng. Sci. 63, 2450–2464.
Hunt, M.L., Zenit, R., Campbell, C.S., Brennen, C.E., 2002. Revisiting the 1954 suspension experiments of R.A. Bagnold. J. Fluid Mech. 452, 1–24.
Johnson, K.L., 1985. Contact Mechanics. Cambridge University Press, Cambridge.
Joseph, G.G., Zenit, R., Hunt, M.L., Rosenwinkel, A.M., 2001. Particle wall collision in a viscous fluid. J. Fluid Mech. 433, 329–346.
Joseph, G.G., Hunt, M.L., 2004. Oblique particle–wall collisions in a liquid. J. Fluid. Mech. 510, 71–93.
Koch, D.L., 1990. Kinetic theory for a monodisperse gas–solid suspension. Phys. Fluids A 2, 1711–1723.
Legendre, D., Zenit, R., Daniel, C., Guiraud, P., 2006. A note on the modelling of the bouncing of spherical drops or solid spheres on a wall in viscous fluid. Chem. Eng. Sci. 61, 3543–3549.
Maw, N., Barber, J.R., Fawcett, J.N., 1976. The oblique impact of elastic spheres. Wear 38, 101–114.
Mindlin, R.D., 1949. Compliance of elastic bodies in contact. Trans. ASME: J. Appl. Mech. 16, 259–268.
Nore, O., 1992. Les lits fluidiss triphasiques destins la biotechnologie utilisant des particules de faible masse volumique. Hydrodynamique, transferts de chaleur et de matire, Ph.D. thesis, Institut National Polytechnique de Lorraine, Vandoeuvre-ls-Nancy, France.
Richardson, J.F., Zaki, W.N., 1954. Sedimentation and fluidisation. Part 1. Trans. Inst. Chem. Eng. 32, 35–53.
Simonin, O., 1991, Prediction of the dispersed phase turbulence in particle-laden jets. In: Proceedings of the 4th International Symposium on Gas–Solid Flows, ASME FED, pp. 121–197.
Walton, O.R., 1993. Numerical simulation of inelastic, frictional particle–particle interactions. In: Roco, M.C. (Ed.), Particulate Two-phase Flow. Butterworth-Heinemann, Oxford.
Wang, J., Ge, W., 2005. Collisional particle-phase pressure in particle–fluid flows at high particle inertia. Phys. Fluids 17, 128103.
Yang, F.-L., Hunt, M.L., 2006. Dynamics of particle–particle collisions in a viscous liquid. Phys. Fluids 18, 121506.
Zenit, R., Hunt, M.L., Brennen, C.E., 1997. Collisional particle pressure measurements in solid–liquid flows. J. Fluid Mech. 353, 261–283.